Supporting Information: Elucidation of the Hydrogen Evolution Reaction on a Photochemical Molecular Device

Miftahussurur Hamidi Putra,[†] Alexander K. Mengele,[‡] Benedikt Bagemihl,[‡] Sven Rau,[‡] Michael Busch,[†,¶,§] and Axel Groß*[,†,∥]

†Institute of Theoretical Chemistry, Ulm University, 89081 Ulm, Germany

‡Institute of Inorganic Chemistry I, Materials and Catalysis, Ulm University, 89081 Ulm, Germany

¶Division of Materials Science, Department of Engineering Sciences and Mathematics, Luleå University of Technology, 971 87 Luleå, Sweden

§Wallenberg Initiative Materials Science for Sustainability (WISE), Luleå University of Technology, 971 87 Luleå, Sweden

∥Helmholtz Institute Ulm (HIU), Electrochemical Energy Storage, 89069 Ulm, Germany

E-mail: axel.gross@uni-ulm.de

S1 Methodology for Calculating pK$_a$

To measure the capability of the intermediates to react with a proton, we calculate here the pK$_a$ using the methodology that was developed by Busch and coworkers.[1–3] The approach is based on a thermodynamic cycle that represents acid dissociation as a sequence of proton-

coupled electron transfer (PCET) oxidation steps.

$$\text{A–H} \longrightarrow \text{A}\cdot + \text{H}^+ + \text{e}^- \tag{S1}$$

and an electron transfer (eT) reduction reaction in the solvent of interest, here is acetonitrile.

$$\text{A}\cdot + \text{e}^- \longrightarrow \text{A}^- \tag{S2}$$

To calculate the electrochemical potential of the electron transfer (eT) step, one needs information about the (effective) absolute potential ($E_{\text{abs,eff}}(\text{SHE})$) that links the absolute reaction energy to the standard hydrogen electrode (SHE) by using equation.

$$E_{\text{abs,eff}}(\text{SHE}) = -nF[0.5G(\text{H}_2) + G(\text{A}^-) - G(\text{A–H}) - \Delta G(\text{Diss.})] \tag{S3}$$

Here, n represents the number of transferred electrons (n=1), F stands for the Faraday constant, and $G(\text{H}_2)$, $G(\text{A}^-)$, and $G(\text{A–H})$ refer to the total Gibbs free energies of hydrogen, the reference acid, and its corresponding base, respectively. These values are obtained from calculations assuming the solvent in which the experimental measurement has been conducted (typically water). Finally, $\Delta G(\text{Diss.})$ is the experimental Gibbs free energy derived from an experimental pK_a measurement in H_2O:

$$\Delta G(\text{Diss.}) = RT[\text{pKa(ref.)}]\ln 10 \tag{S4}$$

with pKa(ref.) here the reference pK_a value from the experimental result. In this work, we use pK_a of formic acid (pKa = 3.77[4]) on water as reference.

Then, leveraging the effective absolute potential, the Gibbs Free energy of the (eT) reduction step ($\Delta G(\text{ET})$) is then determined using equation S5:

$$\Delta G(\text{ET}) = G(\text{A}^-) - G(\text{A}\cdot) + \frac{E_{\text{abs,eff}}(\text{SHE})}{nF} \tag{S5}$$

This method relies on the absolute potential in water. Thus, it will predict the potential versus the SHE in water, despite using the solvation model parameters of the non-aqueous solvent of interest.

This is opposed to the redox potential of the PCET oxidation step ($\Delta G(\mathrm{PCET})$) which is computed using the computational normal hydrogen electrode.[5] This method uses H_2 in the gas phase as a reference.

$$\Delta G(\mathrm{PCET}) = G(\mathrm{A}\cdot) + 0.5G(\mathrm{H_2}) - G(\mathrm{A{-}H}) - RT\ln[\mathrm{H^+}] \tag{S6}$$

The term "$RT\ln([\mathrm{H^+}])$" is derived from the Nernst equation and accounts for the pH dependence of PCET steps. When considering standard conditions (pH = 0), this term equals zero. As the solvent affects the system exclusively through the selected solvation model, the prediction of PCET steps is developed in relation to the Standard Hydrogen Electrode (SHE) in the solvent of interest. Consequently, the Born-Haber cycle, which connects the PCET and (eT) steps with the acid dissociation reaction ($\Delta G(\mathrm{Diss.})$), is no longer solely determined by the sum of the energetics of the electrochemical steps. Instead, it requires an adjustment through a conversion factor to account for the disparities in proton solvation energy between water and the solvent of interest (referred to as "SolvX"). This correction aligns both reactions on the same reference scale in equation S7.

$$\Delta G(\mathrm{Diss.}) = \Delta G(\mathrm{eT}) + \Delta G(\mathrm{PCET}) + \Delta G_{\mathrm{conv.}}^{\mathrm{SHE;SolvX}} \tag{S7}$$

The difference between the reference solvent of the SHE can be exploited to compute the (effective) proton solvation energy in the solvent of interest ("SolvX") via equation S8:

$$\Delta G_{\mathrm{conv.}}^{\mathrm{SHE;SolvX}} = G(\mathrm{A{-}H;SolvX}) - 0.5G(\mathrm{H_2}) - G(\mathrm{A^-;SolvX}) - \frac{E_{\mathrm{abs,eff}}(\mathrm{SHE})}{F} \tag{S8}$$

and equation S9:

$$G_{\text{eff}}^{\text{SolvX}}(\text{H}^+) = 0.6G(\text{H}_2) + \frac{E_{\text{abs,eff}}(\text{SHE})}{F} - \Delta G_{\text{conv.}}^{\text{SHE;SolvX}} \tag{S9}$$

Here, $G(A-H;\text{SolvX})$ and $G(A;\text{SolvX})$ correspond to the total Gibbs free energy of the reference acid from equation S3 in the considered solvent, while $\Delta G_{\text{conv.}}^{\text{SHE;SolvX}}$ is the conversion factor between different solvents. The obtained effective proton solvation energy can then be used to predict the pK_a in the solvent of interest. In this work, we obtained the proton solvation energy -11.19 eV (experiment -11.06 eV[6,7]). Then, the calculated pK_a is determined by this relation[1–3]

$$\text{pK}_\text{a}(\text{calc.}) = 0.75\ \text{pK}_\text{a}(\text{DFT}) + 3.2. \tag{S10}$$

Here, we examined pK_a values for protonation of water, triethylamine (NEt_3), and acetonitrile in acetonitrile. Our DFT calculations revealed that the protonated water (H_3O^+) and acetonitrile (MeCNH^+) had remarkably low pK_a values of -5.4 and -0.8, respectively, making them hindered protonation sites. In contrast, NEt_3H^+ displayed a high pK_a of 17.0 (exp. 18.8[8]), indicating a strong propensity for proton bonding compared to water and acetonitrile. It means, for the photocatalytic process on $[(\text{tbbpy})_2\text{Ru(tpphz)PtI}_2]^{2+}$ (**RuPtI**$_2$; tbbpy = 4,4'-di-tert-butyl-2,2'-bipyridine; tpphz = tetrapyrido[3,2-a: $2', 3' - c : 3''''$-h: $2''', 3'''$-j]phenazine), the pK_a value of the proton bound to the catalyst side of **RuPtI**$_2$ must exceed the pK_a of NEt_3H^+.

S2 Mulliken charge and Spin Density

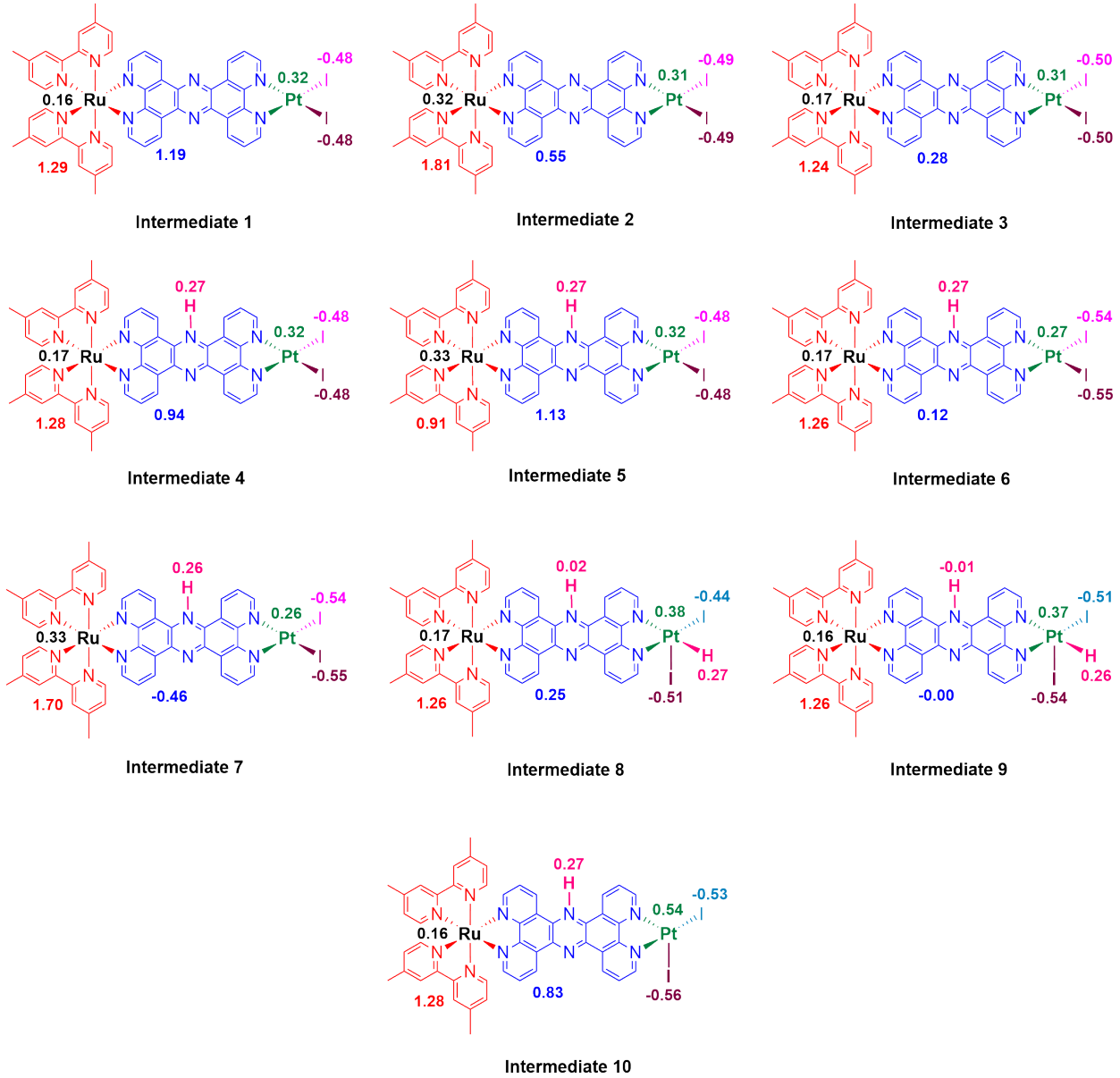

Figure S1: Mulliken charge of the intermediates on the Scheme 1.

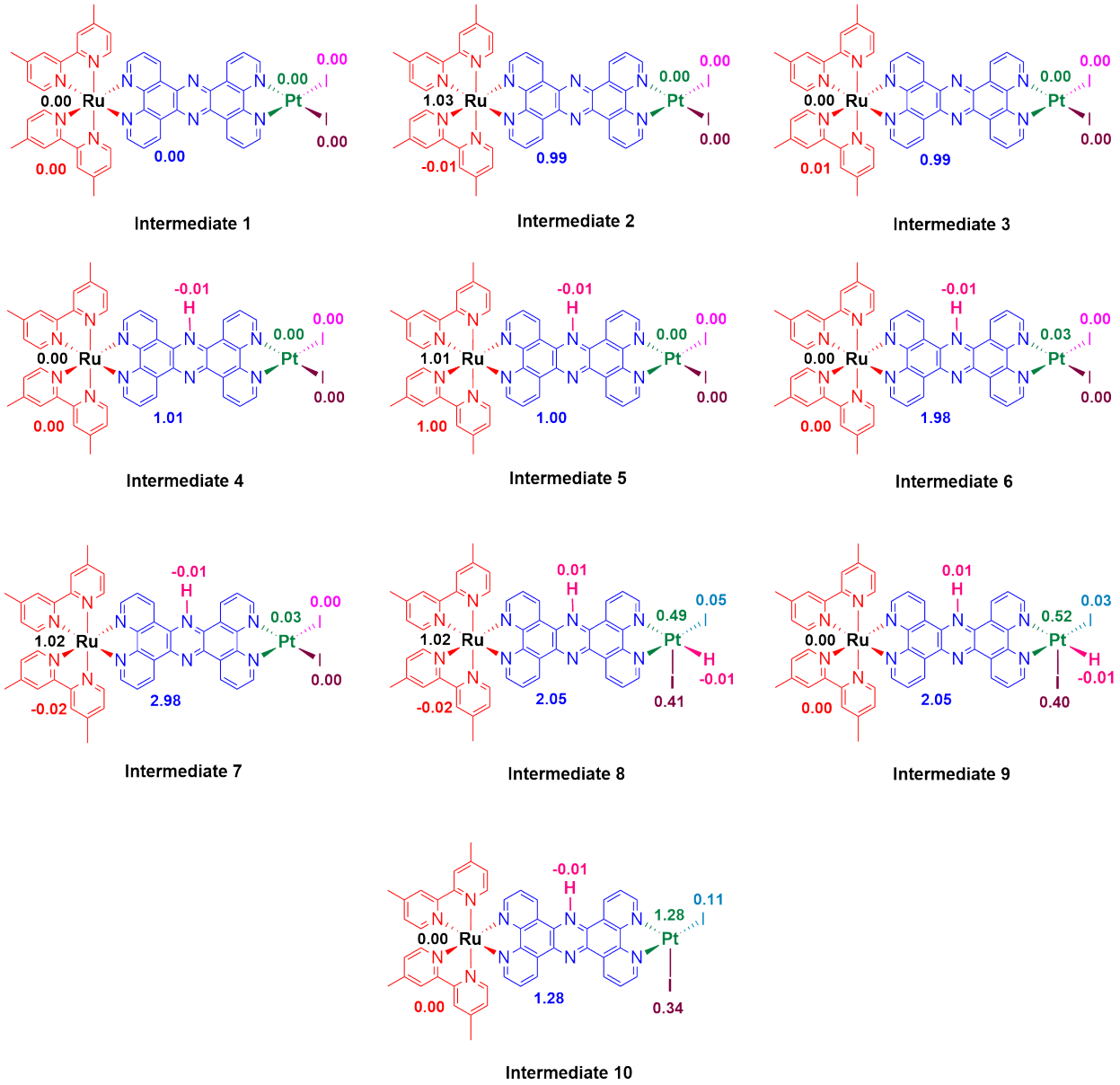

Figure S2: Spin number of the intermediates on the Scheme 1.

S3 The Reaction Energetics

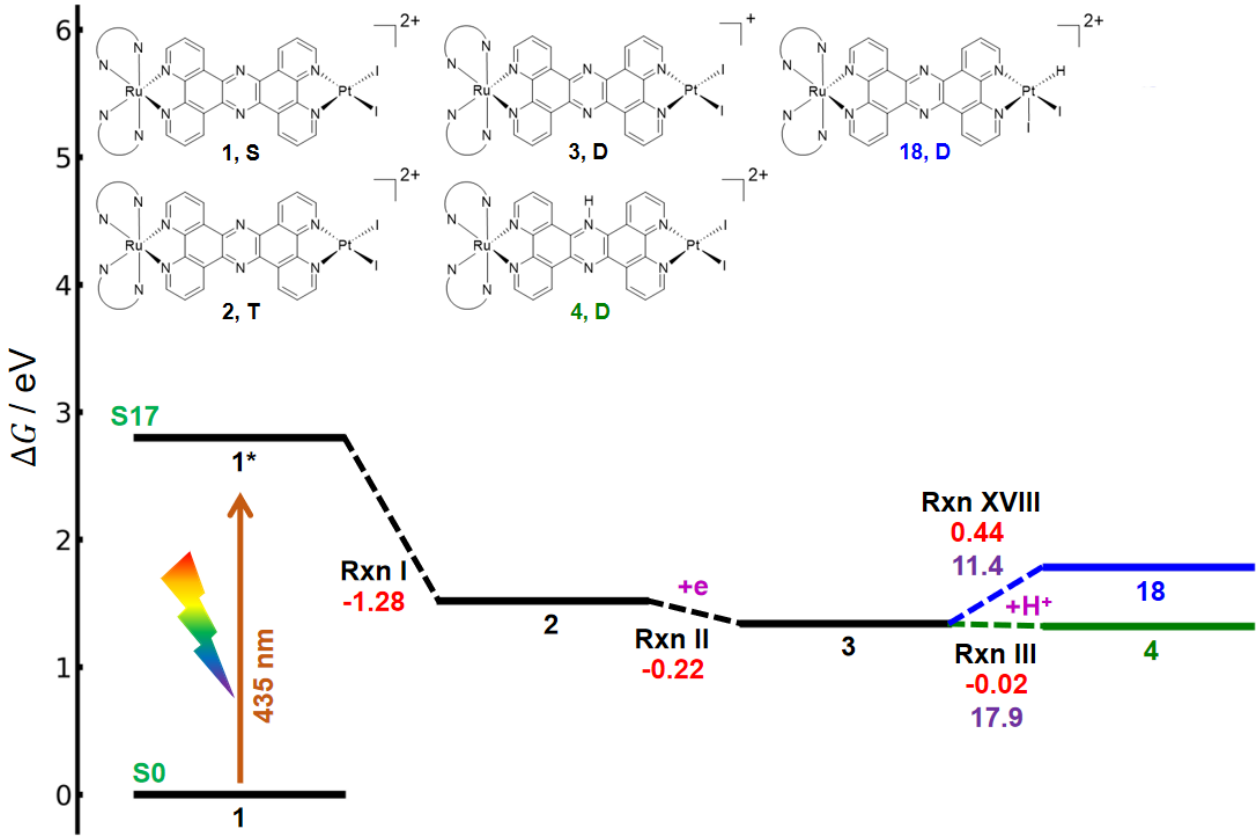

Scheme S1: The reaction energetics on singly reduced doublet state of **RuPtI**$_2$. The number of intermediates and their spin state are written below the molecules with S = singlet, T = triplet, D = doublet. This pK$_a$ calculation is applied to the protonation on the bridging ligand and Platinum catalyst. According to our calculation, the protonation occurs only on the tpphz since the pK$_a$ has a larger value than the pK$_a$ of HNEt$_3^+$ (pK$_a$ = 17.6). Here, the transition state for Rxn III is not displayed and already shown on the manuscript.

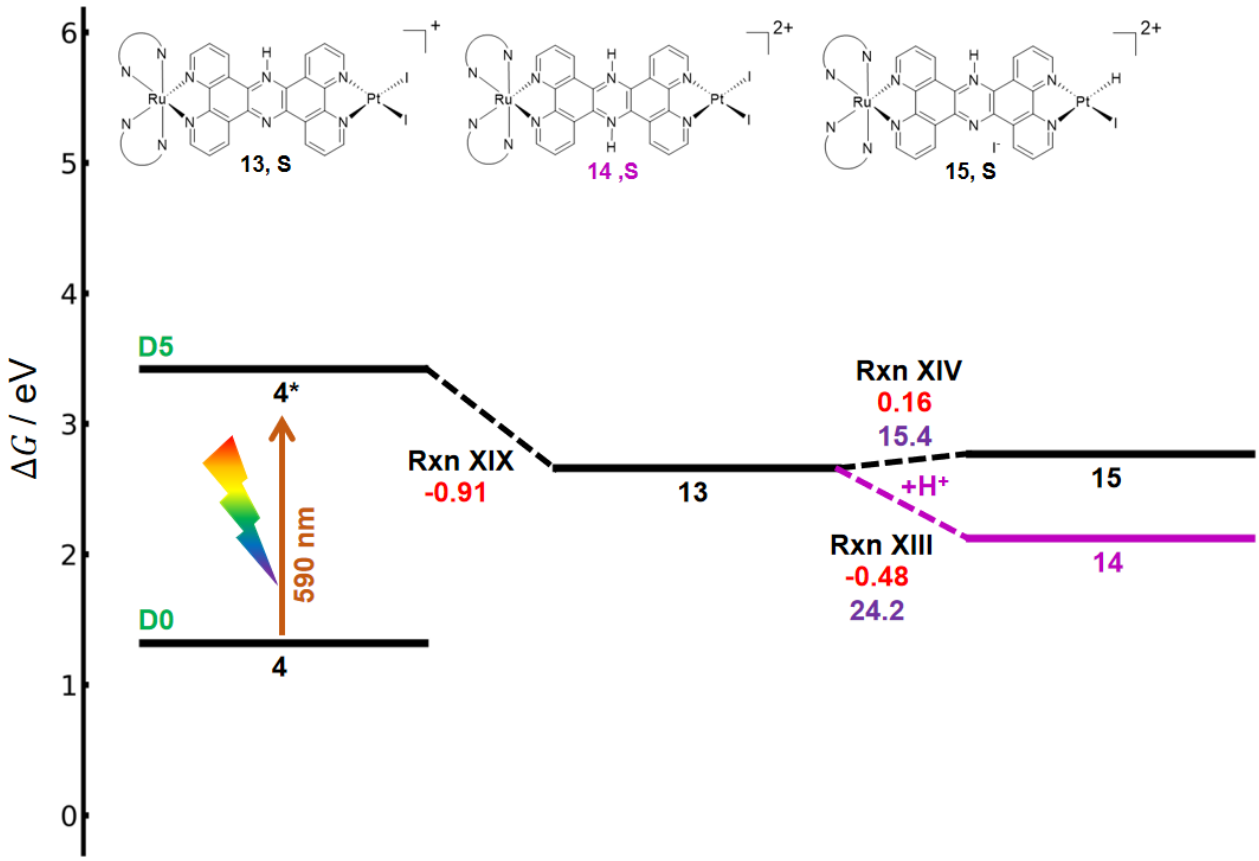

Scheme S2: The reaction energetics of protonation on doubly reduced singlet state of **RuPtI$_2$**. The number of intermediates and their spin state are written below the molecules with S = singlet, D = doublet, and L = loss of I$^-$ ligand. According to our calculation, the second protonation on the bridge has pK$_a$ much larger than pK$_a$ value of HNEt$_3^+$. In addition, protonation on the Pt-catalyst leads to the release of iodide ligand.

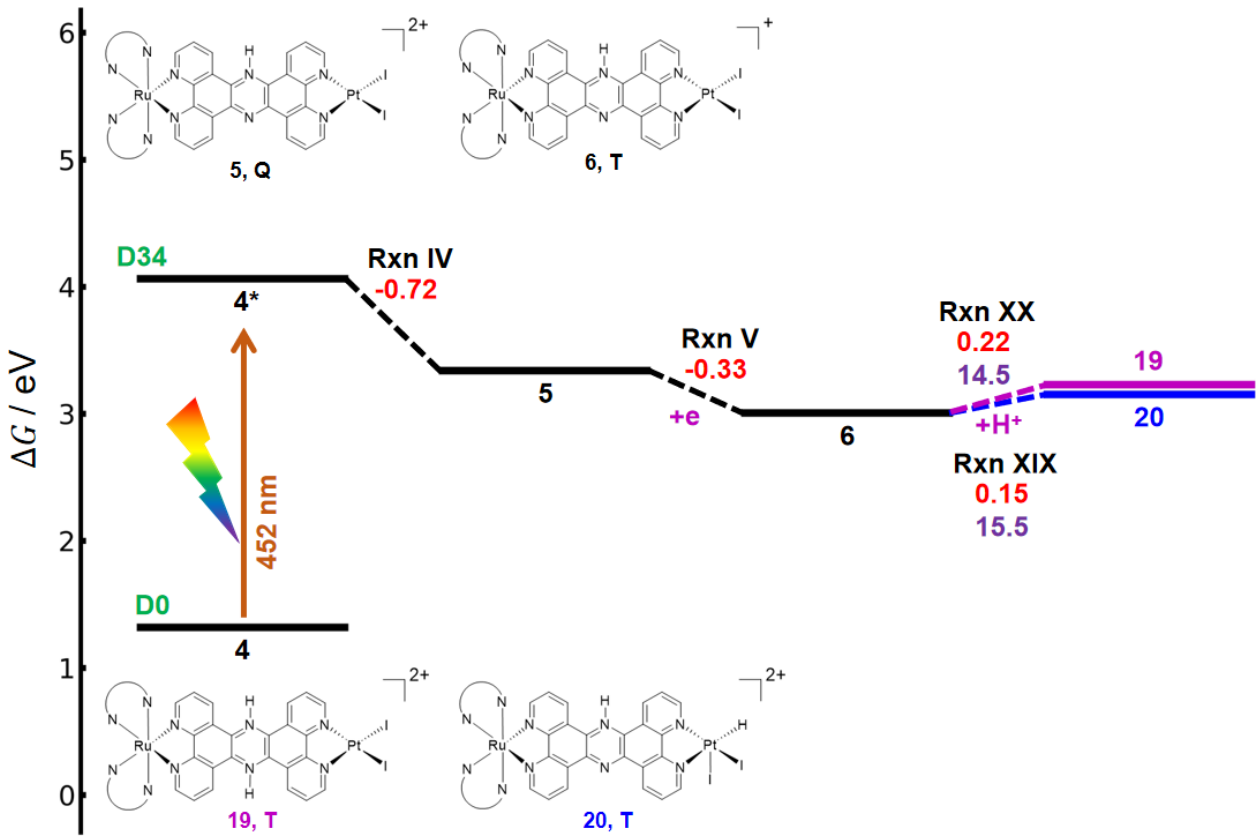

Scheme S3: The reaction energetics of protonation on doubly reduced triplet state of **RuPtI$_2$**. The number of intermediates and their spin state are written below the molecules with T = triplet, D = doublet, and Q = quartet. This calculation is applied to the second protonation on the bridging ligand and first protonation on Pt-catalyst. From our calculation, the pK$_a$ of protonation on both sites are still lower than pK$_a$ value of HNEt$_3^+$ (pK$_a$ = 17.6). Since the pK$_a$ difference is around 2-3 units, therefore the intermediate **19** and **20** may be observed in minor amounts.

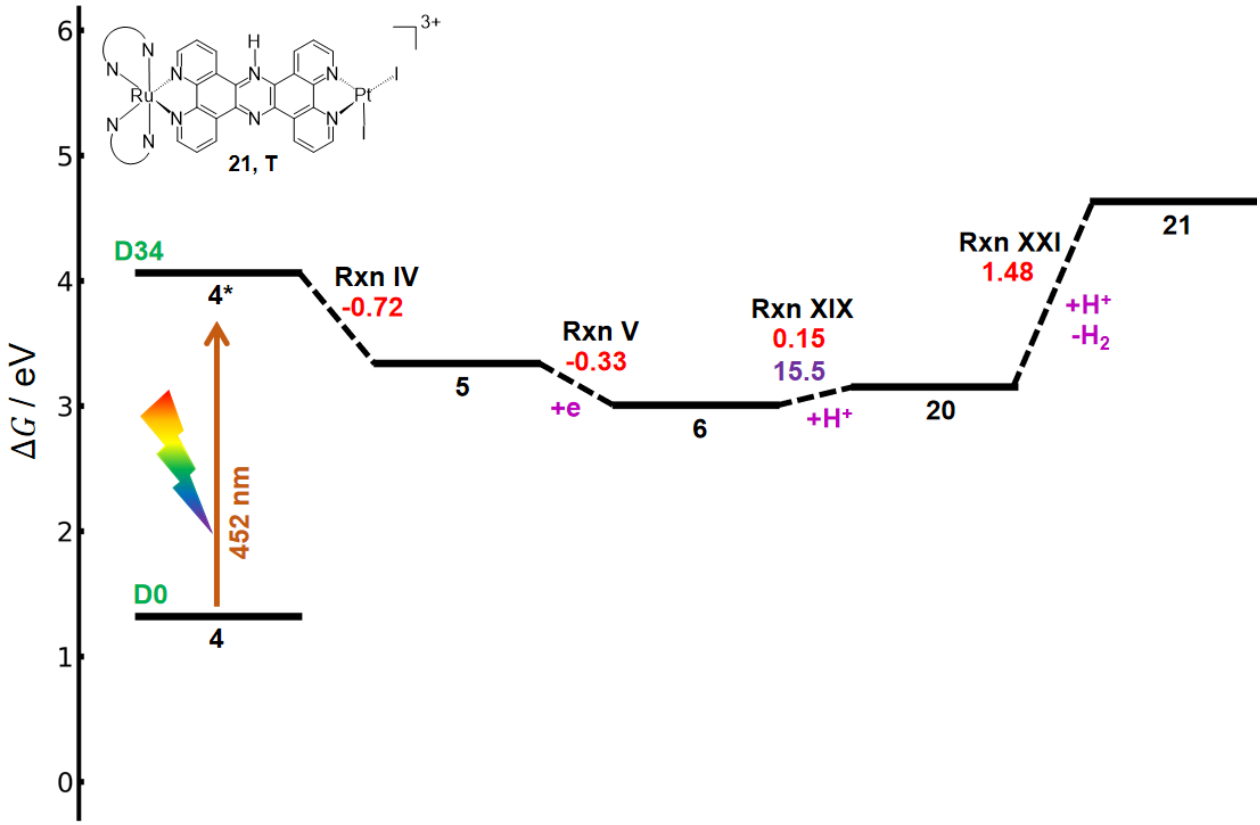

Scheme S4: The reaction energetics plot of the hydrogen production process from doubly reduced triplet state of $\mathbf{RuPtI_2}$. The formation of hydrogen in this figure follows the Volmer-Heyrovsky path. The number of intermediates and their spin state are written below the molecules with T = triplet. According to our calculation, the free energy of hydrogen production is relatively high at a value of 1.48 eV. Therefore, the two-fold reduction process is not effective for hydrogen production.

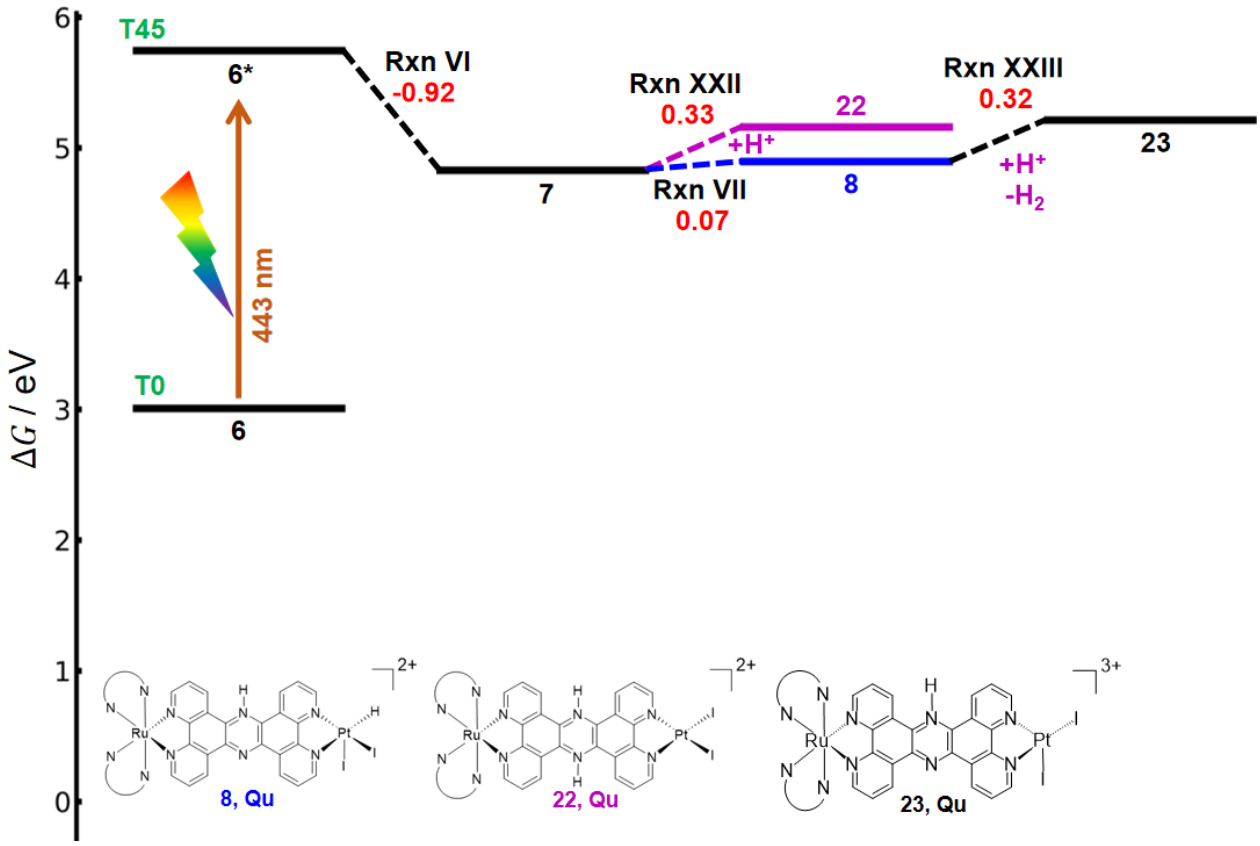

Scheme S5: The reaction energetics plot of the hydrogen production process from doubly reduced quintet state of **RuPtI**$_2$. The formation of hydrogen in this figure follows the Volmer-Heyrovsky path. The number of intermediates and their spin state are written below the molecules with T = triplet and Qu = quintet. Here, the transition state for Rxn VII is not displayed and already shown on the manuscript.

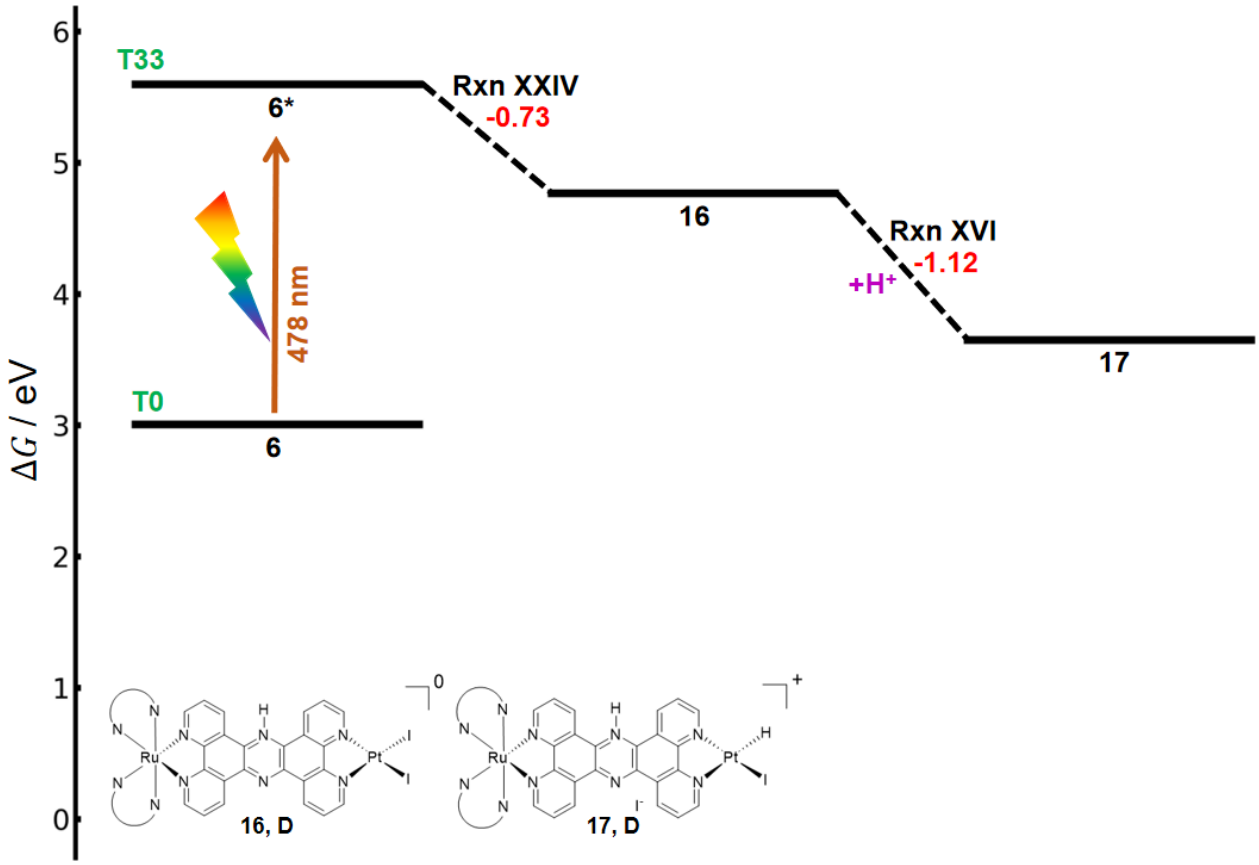

Scheme S6: The reaction energetics of protonation on triply reduced doublet state of **RuPtI**$_2$. The number of intermediates and their spin state are written below the molecules with T = triplet and D = doublet. According to our calculation, the protonation on Pt-catalyst yields the iodide ligand loss.

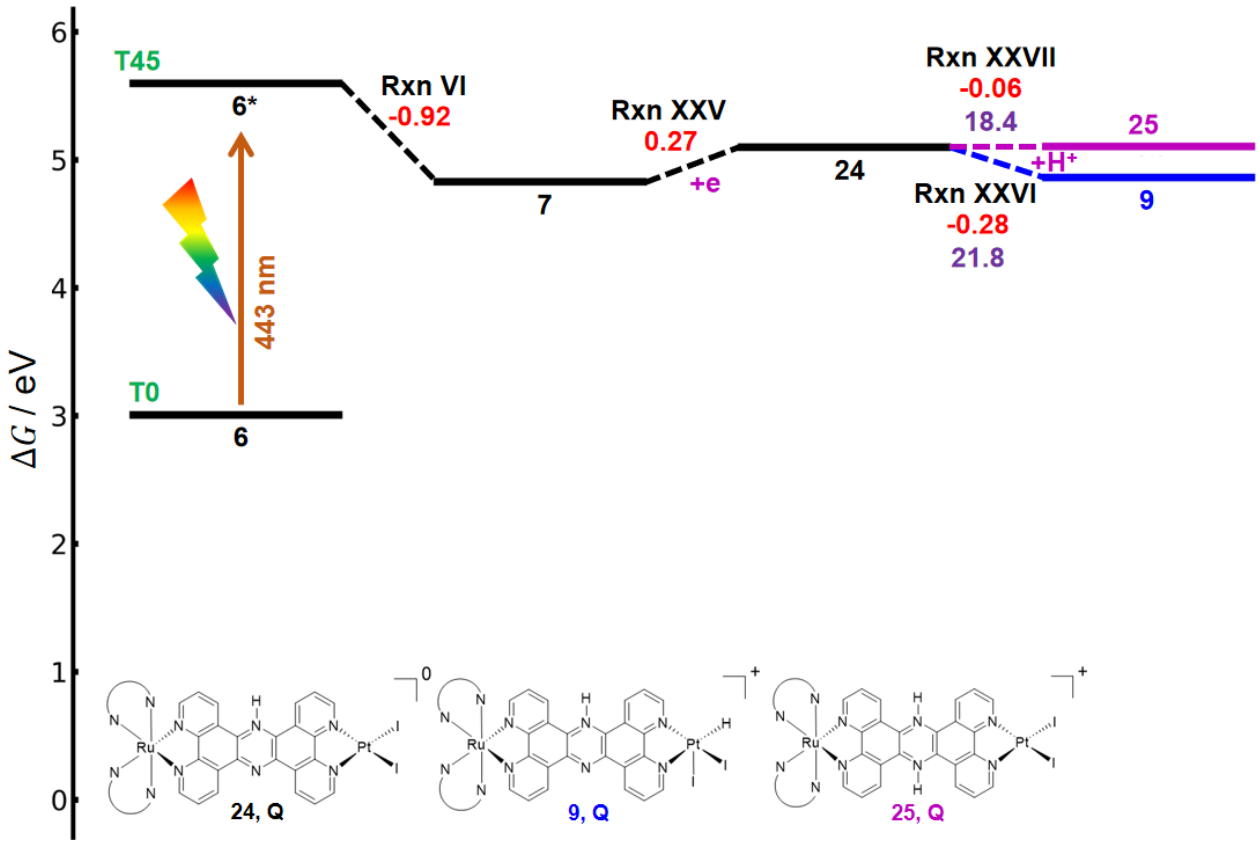

Scheme S7: The reaction energetics of protonation on triply reduced quartet state of **RuPtI**$_2$. The number of intermediates and their spin state are written below the molecules with T = triplet, Q = quartet, and Qu = quintet. This calculation is applied to the second protonation on the bridging ligand and first protonation on Pt-catalyst. From our calculation, the pK$_a$ of protonation on both sites are higher than pK$_a$ value of HNEt$_3^+$ (pK$_a$ = 17.6). Since the pK$_a$ of formation intermediate **9** is three pK$_a$ units higher than the pK$_a$ of formation intermediate **25**, therefore the deactivation process will be slower than the photocatalytic hydrogen evolution reaction.

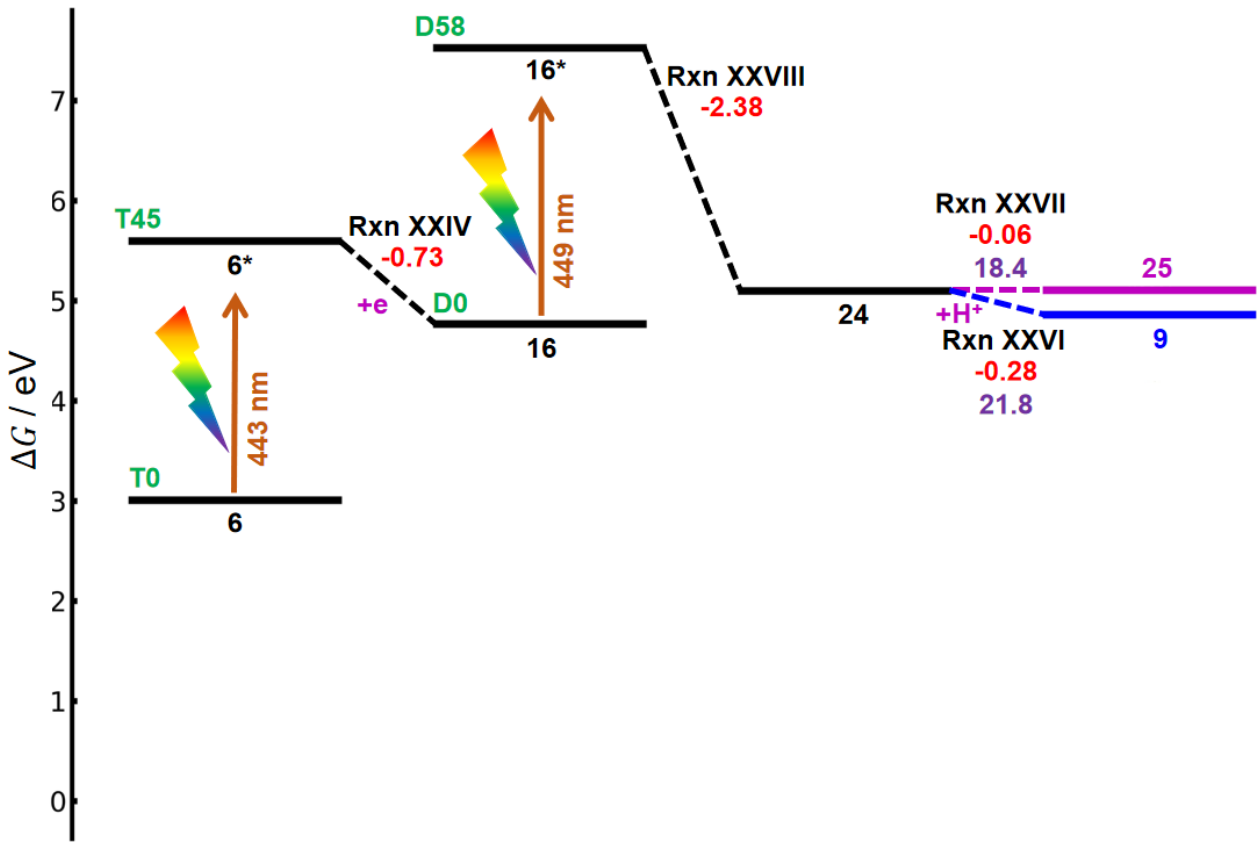

Scheme S8: The reaction energetics of protonation on triply reduced doublet state of $\mathbf{RuPtI_2}$. The number of intermediates and their spin state are written below the molecules with T = triplet and D = doublet. According to our calculation, there is also an alternative due to fast intersystem crossing (ISC) of the $\mathbf{RuPtI_2}$ that can avoid the ligand loss.

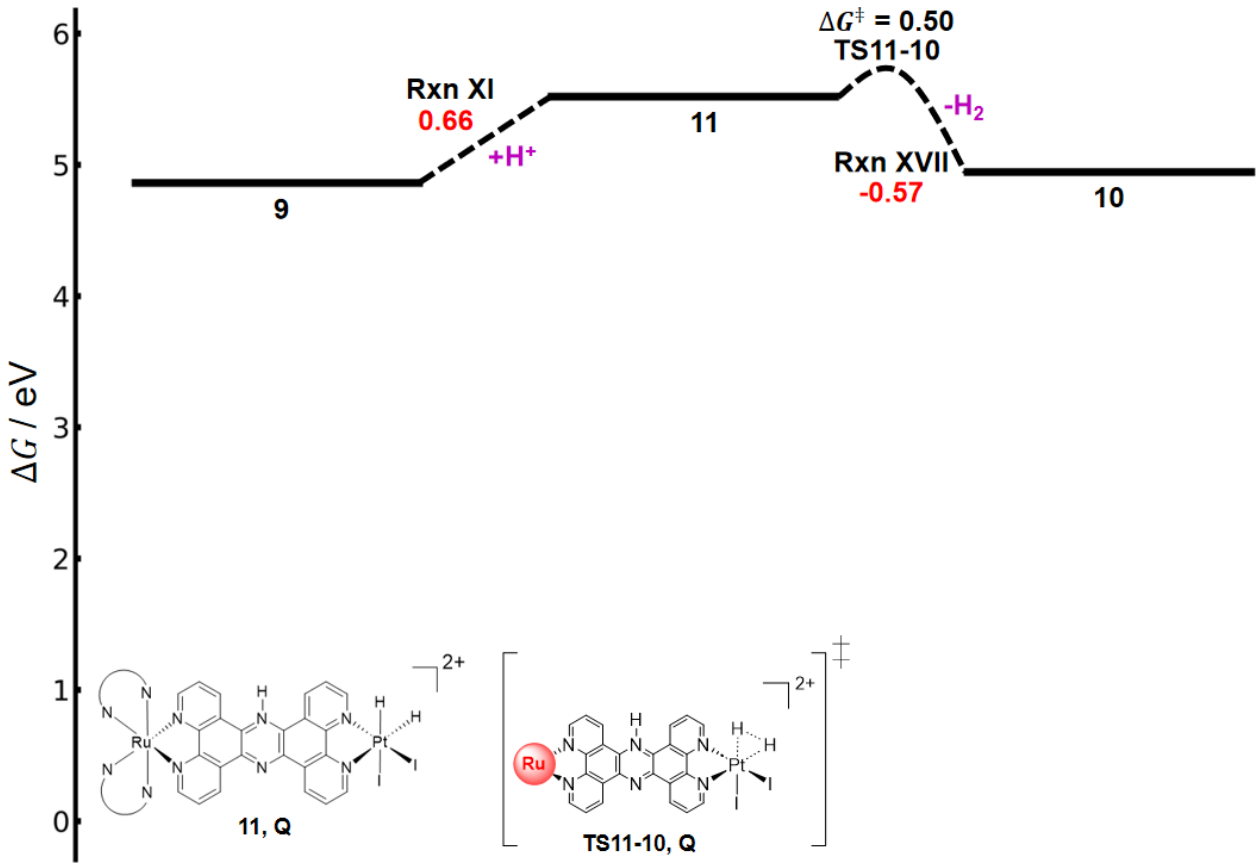

Scheme S9: The reaction energetics plot of hydrogen production process from triply reduced quartet state of $\mathbf{RuPtI_2}$. The formation of hydrogen in this figure follows the Volmer-Tafel path. The number of intermediates and their spin state are written below the molecules with Q = quartet.

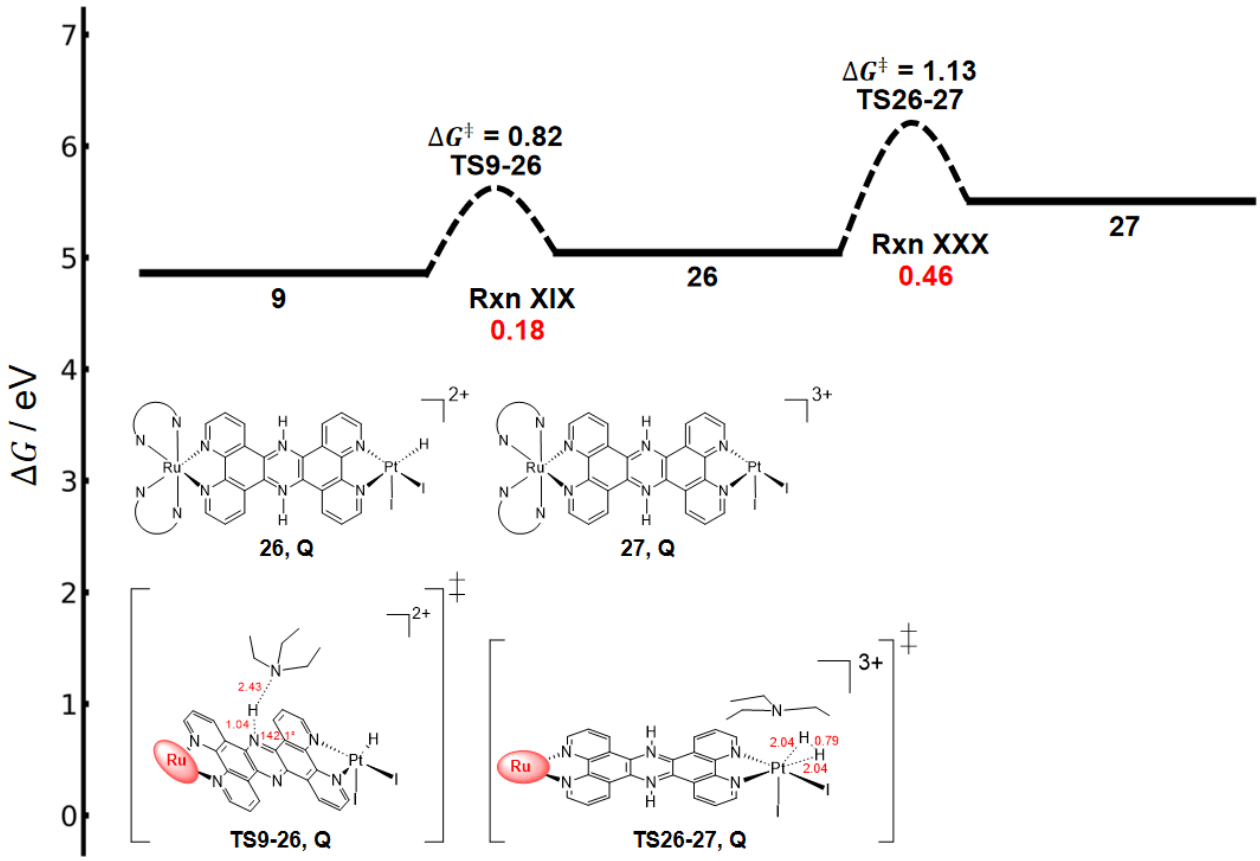

Scheme S10: The reaction energetics plot of deactivation of $\mathbf{RuPtI_2}$ by fully protonated of the bridge on intermediate **9** and hydrogen production of the fully bridge protonated $\mathbf{RuPtI_2}$. The number of intermediates and their spin state are written below the molecules with Q = quartet.

S4 Important Excitation States

S4.1 Intermediate 1

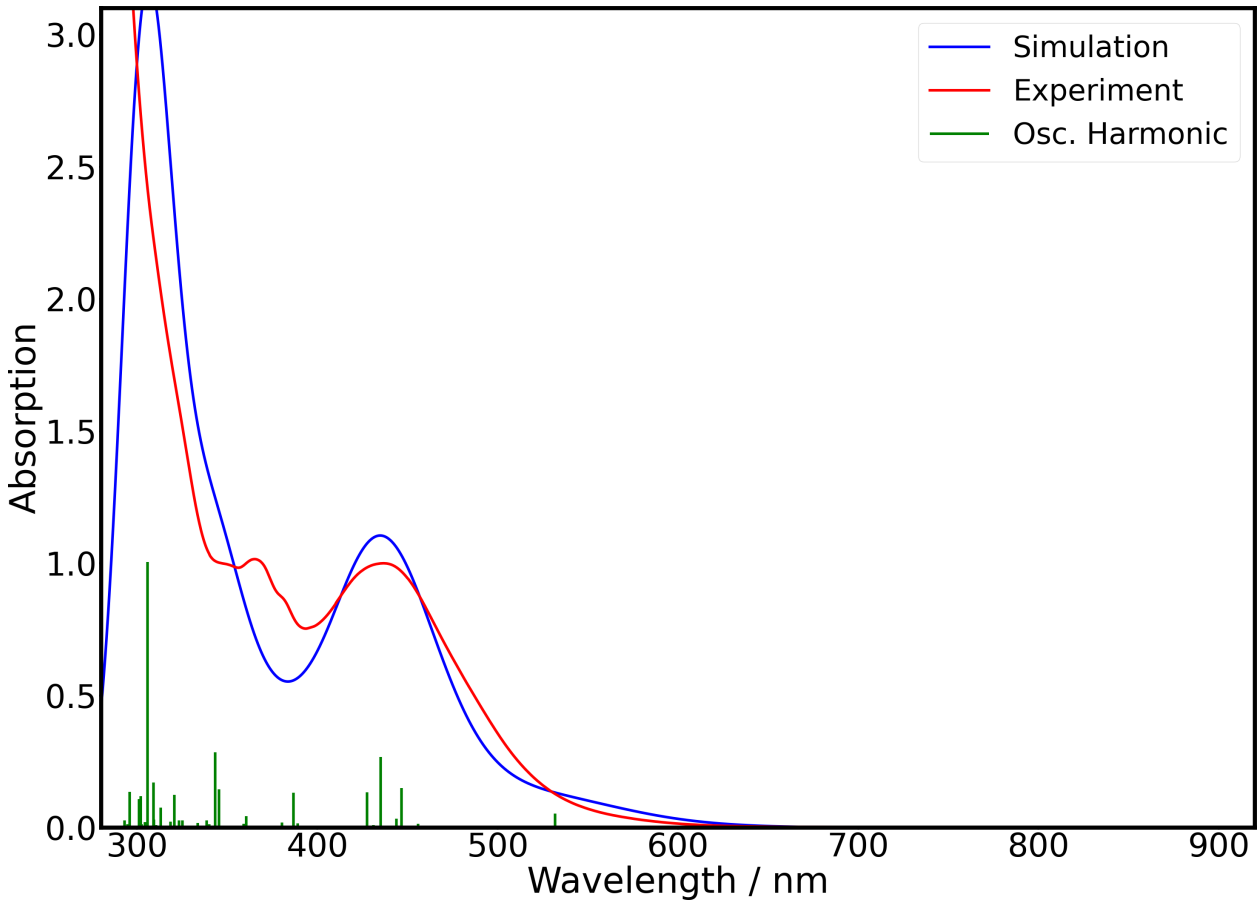

Figure S3: Absorption spectrum of intermediate **1**.

Table S1: Molecular orbital transition of notable singlet-singlet excitation state from TDDFT result on Intermediate **1**. The direction of electron excitation is from red to green.

State	**Transition**	**Orbital Transition**	**%**	**VEE (eV)**	**λ (nm)**	**f**
S2	236 → 239	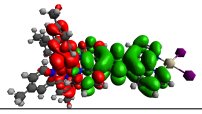	95.82	2.33	531.78	0.0534
S13	236 → 242	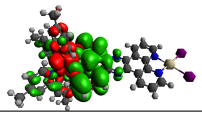	59.81	2.78	446.78	0.1491
	236 → 243	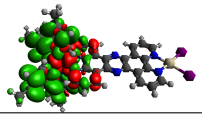	31.72			
S17	233 → 239	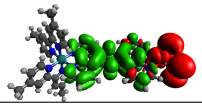	19.97	2.85	435.04	0.2676
	236 → 243	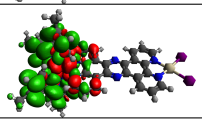	29.67			
	237 → 244	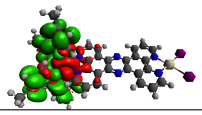	32.52			
	236 → 242	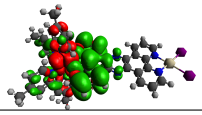	10.07			
S20	236 → 244	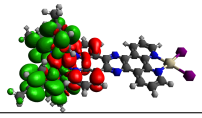	57.67	2.90	427.64	0.1330
	237 → 243	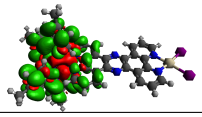	39.09			
S33	233 → 241	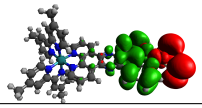	80.20	3.21	386.72	0.1314
	235 → 240	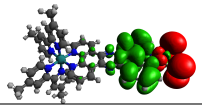	13.58			

Table S2: Molecular orbital transition of notable singlet-triplet excitation state from TDDFT result on Intermediate **1**. The direction of electron excitation is from red to green.

State	**Transition**	**Orbital Transition**	**%**	**VEE (eV)**	**λ (nm)**	**f**
T1	238 → 239	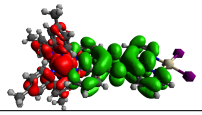	67.78	2.11	588.81	0.0000
	238 → 242	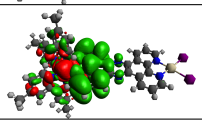	22.80			
T6	235 → 245	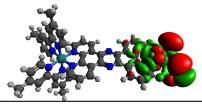	85.79	2.33	531.61	0.0000
T7	238 → 244	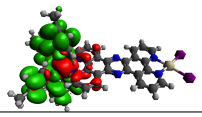	74.48	2.40	516.95	0.0000
T22	235 → 239	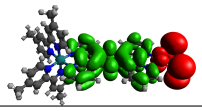	34.77	2.75	449.50	0.0000
	235 → 241	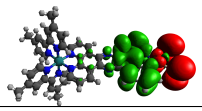	16.27			
T43	238 → 245	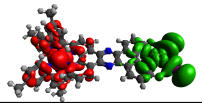	99.94	3.36	368.48	0.0000

S4.2 Intermediate 3

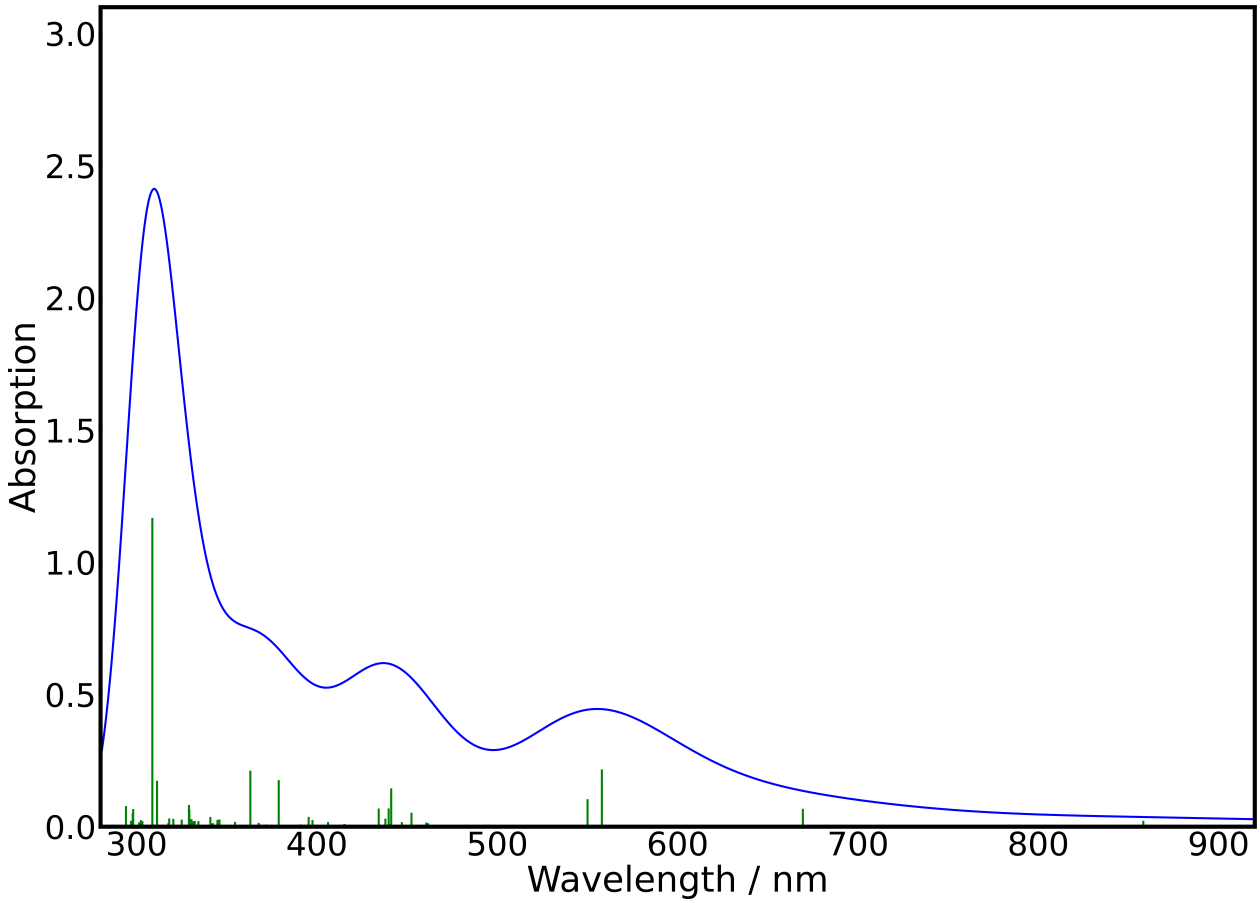

Figure S4: Absorption spectrum of intermediate **3**.

Table S3: Molecular orbital transition of notable excitation state from TDDFT result on Intermediate **3**. The direction of electron excitation is from red to green.

State	Transition	Orbital Transition	%	VEE (eV)	λ (nm)	f
D6	239A → 245A	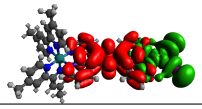	99.67	1.19	1043.43	0.0000
D8	239A → 247A	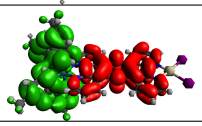	97.27	1.85	669.44	0.0674
D10	239A → 249A	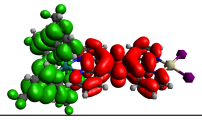	39.63	2.22	557.96	0.2169
	239A → 251A	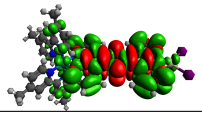	55.91			
D11	239A → 249A	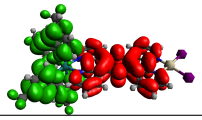	59.21	2.25	550.06	0.1041
	239A → 251A	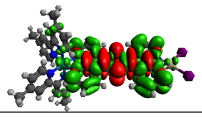	39.37			
D35	237A → 244A	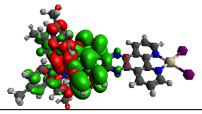	18.42	2.81	441.16	0.1450
	237B → 239B	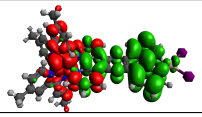	18.20			
	237B → 241B	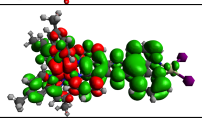	15.29			
D76	238A → 245A	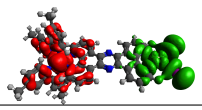	98.28	3.38	367.22	0.0000

S4.3 Intermediate 4

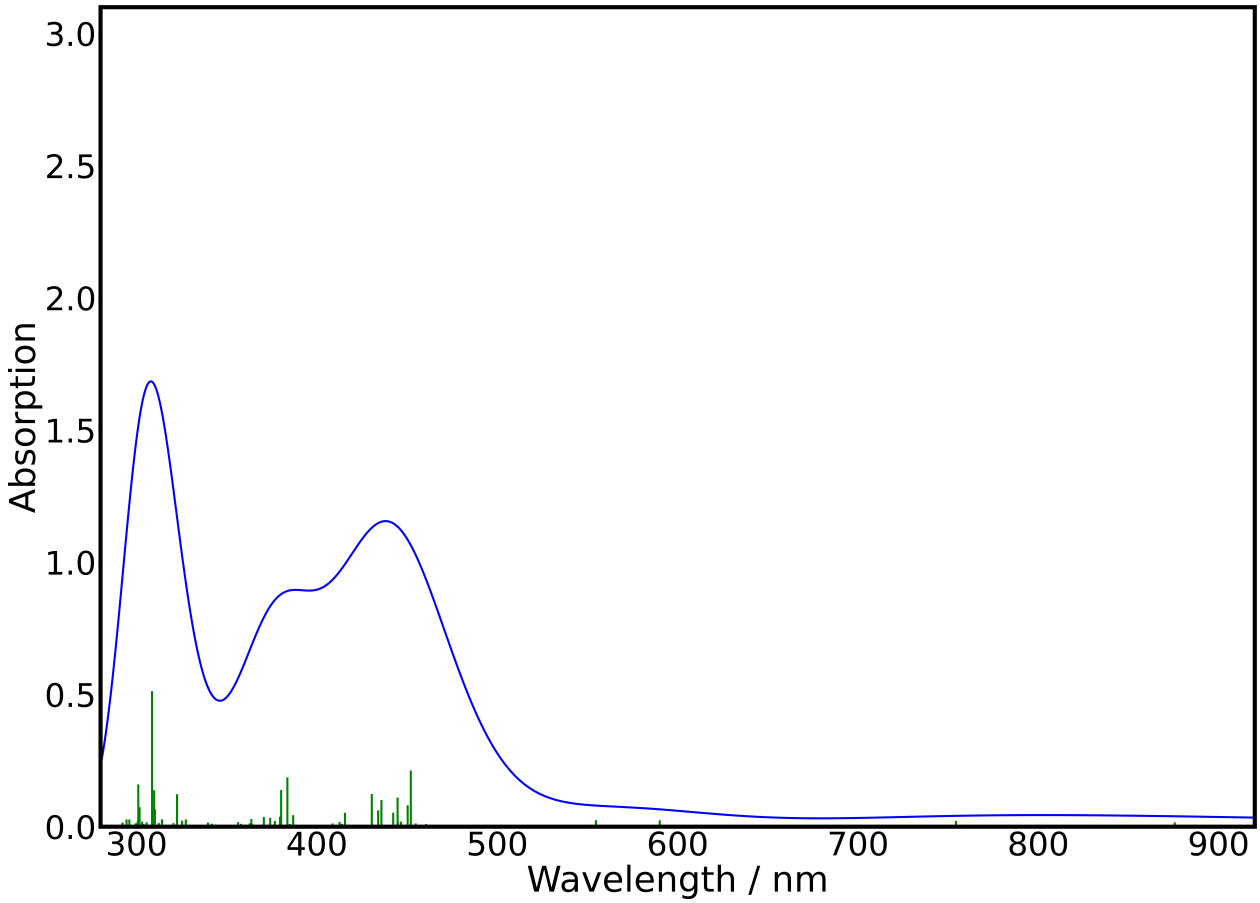

Figure S5: Absorption spectrum of intermediate **4**.

Table S4: Molecular orbital transition of notable excitation state from TDDFT result on Intermediate **4**. The direction of electron excitation is from red to green.

State	Transition	Orbital Transition	%	VEE (eV)	λ (nm)	f
D5	239A → 246A	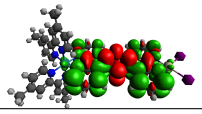	74.64	2.10	590.02	0.0241
D7	239A → 245A	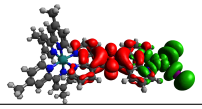	98.43	2.17	571.99	0.0000
D9	236B → 239B	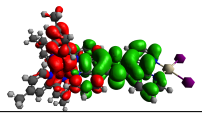	72.39	2.24	554.63	0.0246
D34	236A → 242A	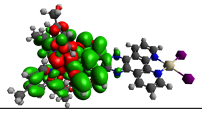	15.94	2.74	452.06	0.2127
	236B → 241B	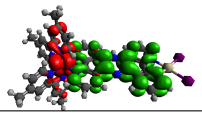	10.88			
	236B → 242B	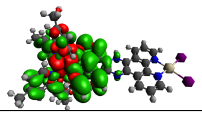	22.10			
D35	236A → 244A	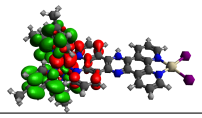	15.53	2.76	450.27	0.0811
	237A → 243A	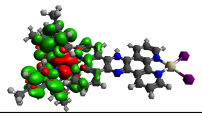	14.81			
	237B → 243B	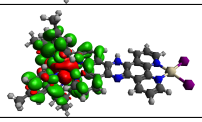	11.33			
D86	238A → 245A	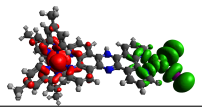	99.15	3.37	367.89	0.0000

S4.4 Intermediate 6

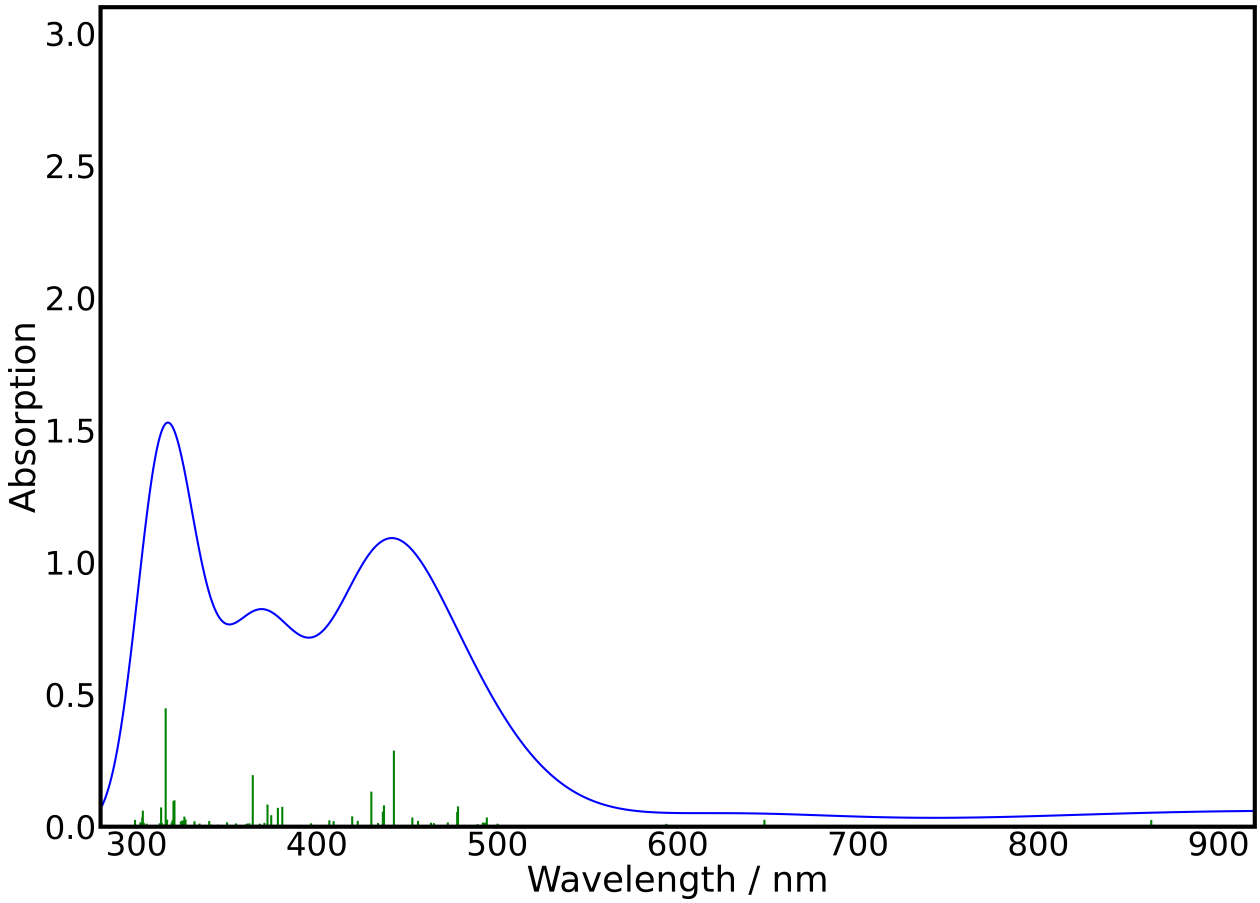

Figure S6: Absorption spectrum of intermediate **6**.

Table S5: Molecular orbital transition of notable excitation state from TDDFT result on Intermediate **6**. The direction of electron excitation is from red to green.

State	Transition	Orbital Transition	%	VEE (eV)	λ (nm)	f
T2	240A → 245A	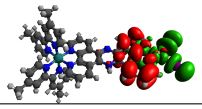	98.13	0.81	1530.43	0.0000
T18	239A → 245A	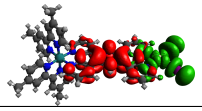	98.03	2.30	539.30	0.0000
T33	237A → 241A	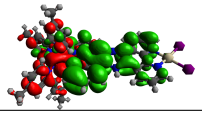	16.46	2.59	478.21	0.0769
	237A → 242A	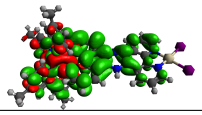	10.09			
	239A → 247A	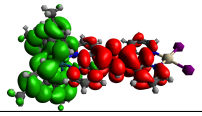	40.60			
T45	233B → 239B	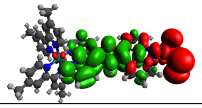	38.55	2.80	442.68	0.2876
	237B → 241B	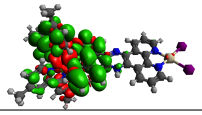	10.00			
T47	238B → 243B	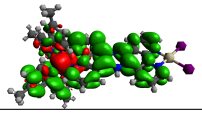	21.25	2.84	437.19	0.0811
T50	237A → 241A	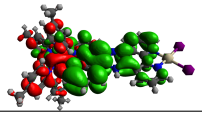	21.64	2.88	430.18	0.1324
	237A → 242A	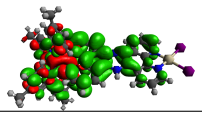	16.28			
	237A → 244A	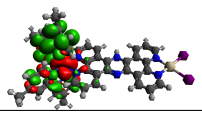	18.88			
T136	238A → 245A	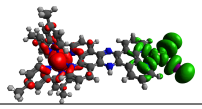	99.84	3.76	330.14	0.0000

S4.5 Intermediate 7

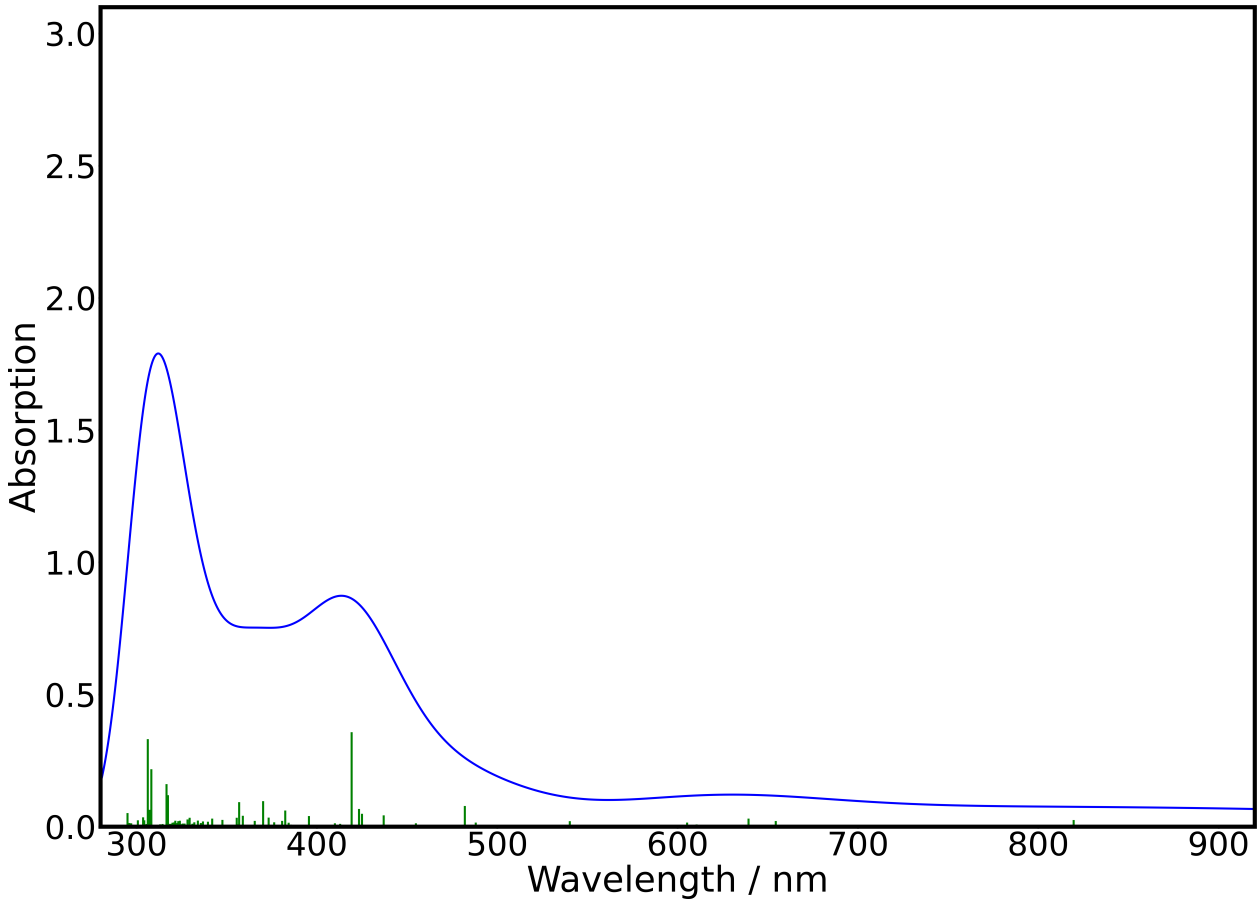

Figure S7: Absorption spectrum of intermediate **7**.

Table S6: Molecular orbital transition of notable excitation state from TDDFT result on Intermediate **7**. The direction of electron excitation is from red to green.

State	**Transition**	**Orbital Transition**	**%**	**VEE (eV)**	**λ (nm)**	**f**
Qu8	241A → 246A	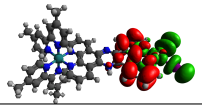	97.79	0.88	1414.59	0.0000
Qu24	240A → 246A	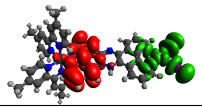	95.11	1.96	633.97	0.0000
Qu30	241A → 253A	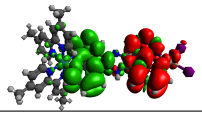	34.90	1.94	639.34	0.0306
	241A → 254A	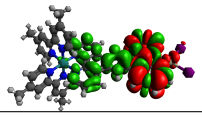	49.87			
Qu37	239A → 246A	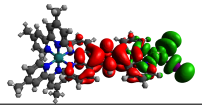	97.26	2.43	509.81	0.0000
Qu47	240A → 255A	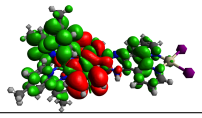	19.09	2.57	482.00	0.0783
	240A → 256A	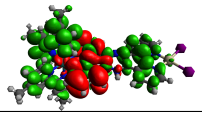	46.73			
Qu60	239A → 252A	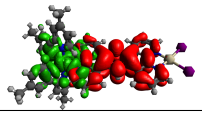	34.82	2.96	419.22	0.3576
	239A → 253A	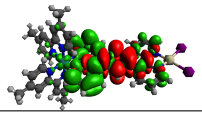	32.78			

S4.6 Intermediate 13

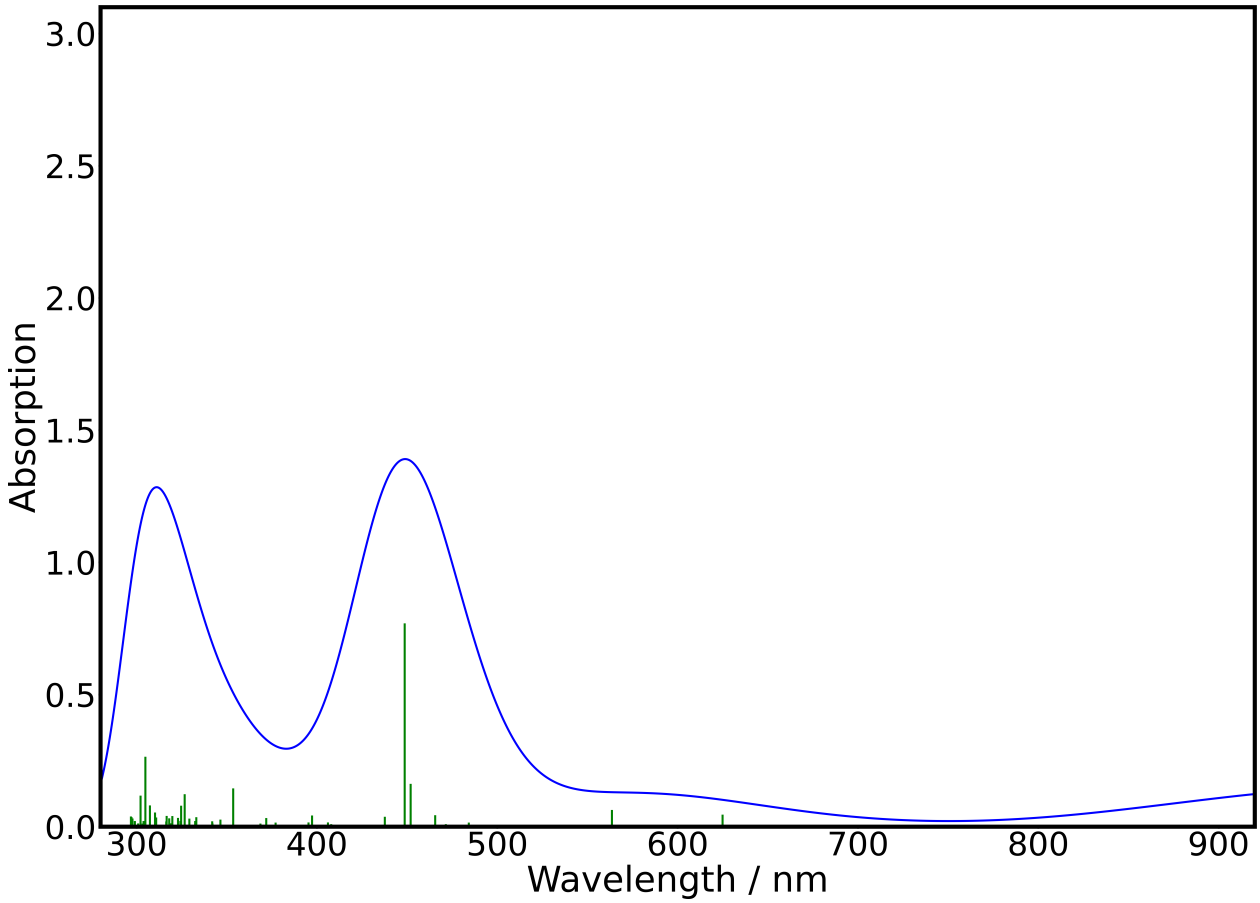

Figure S8: Absorption spectrum of intermediate **13**.

Table S7: Molecular orbital transition of notable excitation state from TDDFT result on intermediate **13**. The direction of electron excitation is from red to green.

State	**Transition**	**Orbital Transition**	**%**	**VEE (eV)**	**λ (nm)**	**f**
S1	239 → 240	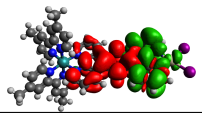	98.80	1.07	1154.36	0.0238
S2	239 → 242	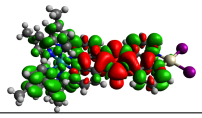	35.09	1.23	1010.48	0.0947
	239 → 243	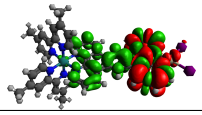	62.61			
S17	236 → 241	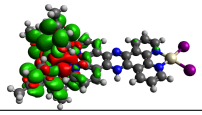	55.78	2.74	451.94	0.1619
	237 → 242	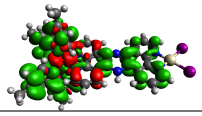	23.12			
S18	236 → 242	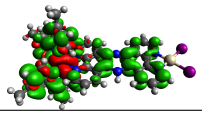	14.77	2.76	448.69	0.7694
	239 → 251	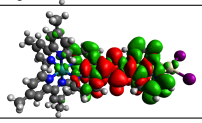	66.40			

S4.7 Intermediate 16

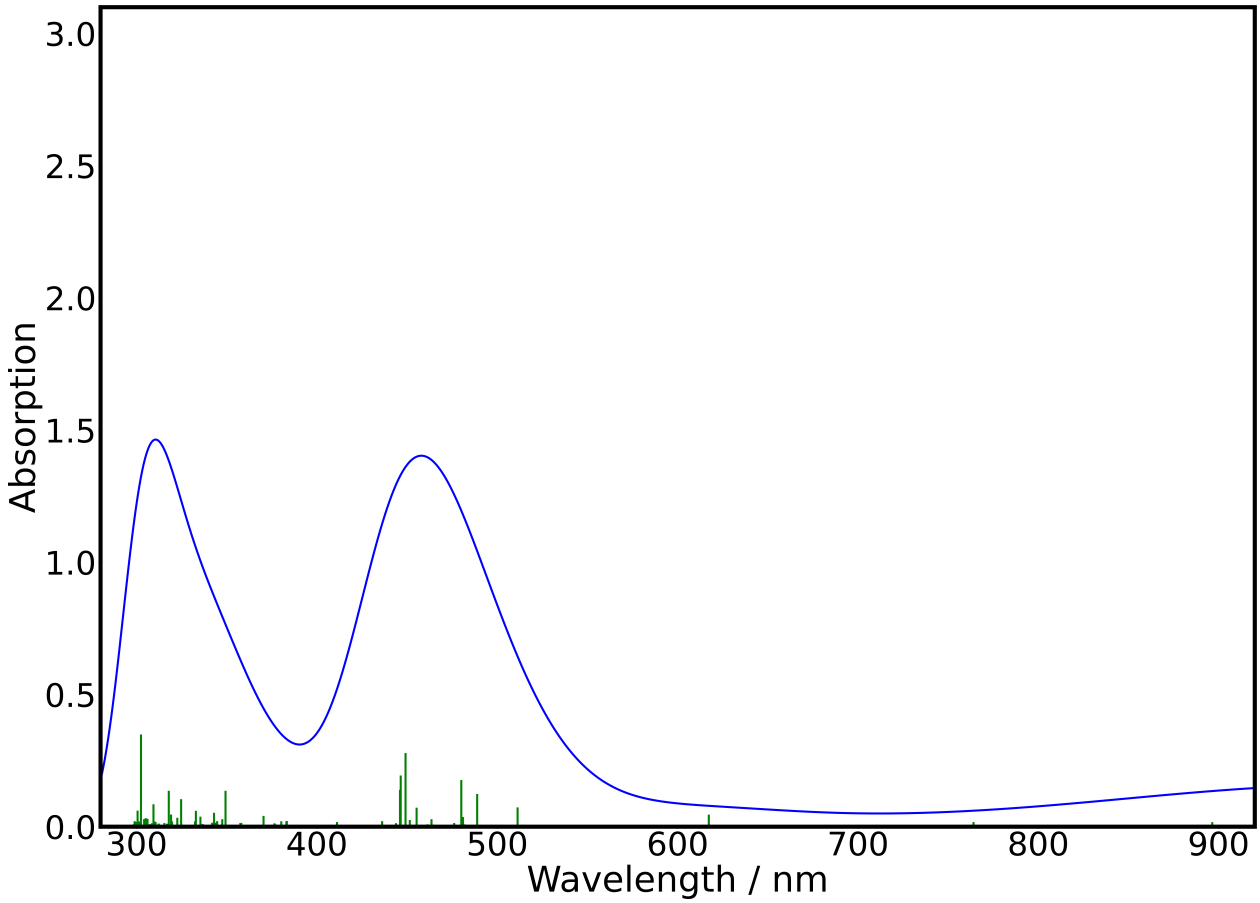

Figure S9: Absorption spectrum of intermediate **16**.

Table S8: Molecular orbital transition of notable excitation state from TDDFT result on intermediate **16**. The direction of electron excitation is from red to green.

State	Transition	Orbital Transition	%	VEE (eV)	λ (nm)	f
D7	240A → 244A	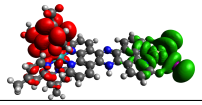	99.89	0.86	1434.92	0.0000
D41	237A → 242A	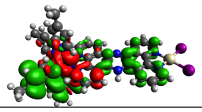	12.88	2.54	488.86	0.1241
	237A → 245A	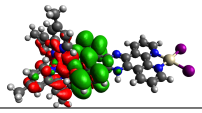	14.65			
	236B → 242B	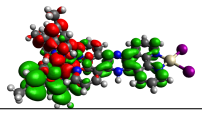	15.71			
D45	236A → 245A	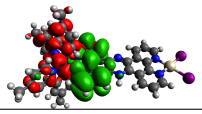	12.11	2.58	480.04	0.1767
	240A → 254A	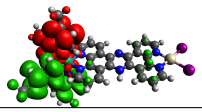	34.94			
	240A → 256A	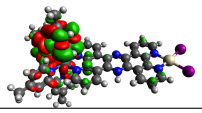	13.31			
D58	236B → 240B	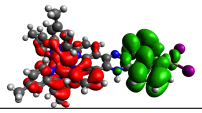	20.91	2.76	449.12	0.2786
D59	236A → 241A	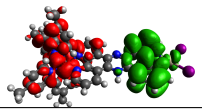	13.97	2.78	446.41	0.1939
	236A → 243A	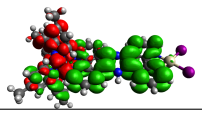	26.55			
	239A → 249A	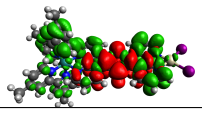	11.68			
D60	236B → 240B	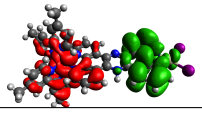	48.25	2.78	446.09	0.1393

S5 Coordinate of Intermediates

All optimized equilibrium structures of all intermediates can be found via the open repository Zenodo https://doi.org/10.5281/zenodo.10457987.[9]

References

(1) Busch, M.; Ahlberg, E.; Ahlberg, E.; Laasonen, K. How to Predict the pK_a of Any Compound in Any Solvent. *ACS Omega* **2022**, *7*, 17369–17383.

(2) Busch, M.; Ahlberg, E.; Laasonen, K. Universal Trends between Acid Dissociation Constants in Protic and Aprotic Solvents. *Chem. Eur. J.* **2022**, *28*.

(3) Busch, M.; Ahlberg, E.; Laasonen, K. From absolute potentials to a generalized computational standard hydrogen electrode for aqueous and non-aqueous solvents. *Phys. Chem. Chem. Phys.* **2021**, *23*, 11727–11737.

(4) Rumble, J., Ed. *CRC handbook of chemistry and physics*, 104th ed.; CRC Handbook of Chemistry and Physics; CRC Press: London, England, 2023.

(5) Nørskov, J. K.; Rossmeisl, J.; Logadottir, A.; Lindqvist, L.; Kitchin, J. R.; Bligaard, T.; Jónsson, H. Origin of the Overpotential for Oxygen Reduction at a Fuel-Cell Cathode. *J. Phys. Chem. B* **2004**, *108*, 17886–17892.

(6) Muckerman, J. T.; Skone, J. H.; Ning, M.; Wasada-Tsutsui, Y. Toward the accurate calculation of pKa values in water and acetonitrile. *Biochim. Biophys. Acta* **2013**, *1827*, 882–891.

(7) Rossini, E.; Knapp, E.-W. Proton solvation in protic and aprotic solvents. *J. Comput. Chem.* **2016**, *37*, 1082–1091.

(8) Tshepelevitsh, S.; Kütt, A.; Lõkov, M.; Kaljurand, I.; Saame, J.; Heering, A.; Plieger, P. G.; Vianello, R.; Leito, I. On the Basicity of Organic Bases in Different Media. *European Journal of Organic Chemistry* **2019**, *2019*, 6735–6748.

(9) Putra, M. H.; Rau, S.; Groß, A.; Busch, M. *The Relaxed Geometry of Intermediates from Photocatalytic Hydrogen Evolution Reaction of RuPtI2 Photocatalyst*; Zenodo, 2024; https://doi.org/10.5281/zenodo.10457987.